Imaging the ramp–décollement geometry of the Chelungpu fault using coseismic GPS displacements from the 1999 Chi-Chi, Taiwan earthquake

Kaj M. Johnson*, Paul Segall

Geophysics Department, Stanford University, 397 Panama Mall, Mitchel 313, Stanford, CA 94305-2215, USA

Abstract

We use coseismic GPS data from the 1999 Chi-Chi, Taiwan earthquake to estimate the subsurface shape of the Chelungpu fault that ruptured during the earthquake. Studies prior to the earthquake suggest a ramp–décollement geometry for the Chelungpu fault, yet many finite source inversions using GPS and seismic data assume slip occurred on the down-dip extension of the Chelungpu ramp, rather than on a sub-horizontal décollement. We test whether slip occurred on the décollement or the down-dip extension of the ramp using well-established methods of inverting GPS data for geometry and slip on faults represented as elastic dislocations. We find that a significant portion of the coseismic slip did indeed occur on a sub-horizontal décollement located at ~ 8 km depth. The slip on the décollement contributes 21% of the total modeled moment release. We estimate the fault geometry assuming several different models for the distribution of elastic properties in the earth: homogeneous, layered, and layered with lateral material contrast across the fault. It is shown, however, that heterogeneity has little influence on our estimated fault geometry. We also investigate several competing interpretations of deformation within the E/W trending rupture zone at the northern end of the 1999 ground ruptures. We demonstrate that the GPS data require a 22- to 35-km-long lateral ramp at the northern end, contradicting other investigations that propose deformation is concentrated within 10 km of the Chelungpu fault. Lastly, we propose a simple tectonic model for the development of the lateral ramp.
© 2003 Elsevier B.V. All rights reserved.

Keywords: Décollement; GPS; Taiwan; Geodetic inversion; Fault slip

1. Introduction

The 1999 Chi-Chi, Taiwan earthquake ($M_w = 7.6$) nucleated at 8–10 km depth and propagated to the surface generating 100 km of ground rupture, extending 80 km north/south from Chushan to Fengyuan and 20 km east/west from Fengyuan to Shuangchi (Fig. 1; Kao et al., 2000). The 80-km Chushan–Fengyuan section ruptured part of the previously recognized Chelungpu fault. Surface features such as ground ruptures and folding along this segment are consistent with reverse/left-lateral fault dipping ~ 30° east. The ground ruptures deviate from the trend of the Chelungpu fault at the northern end in the east/west Fengyuan–Shuangchi section where rupture occurred in a 3-km-wide zone consisting of six segments of north and south dipping reverse faults.
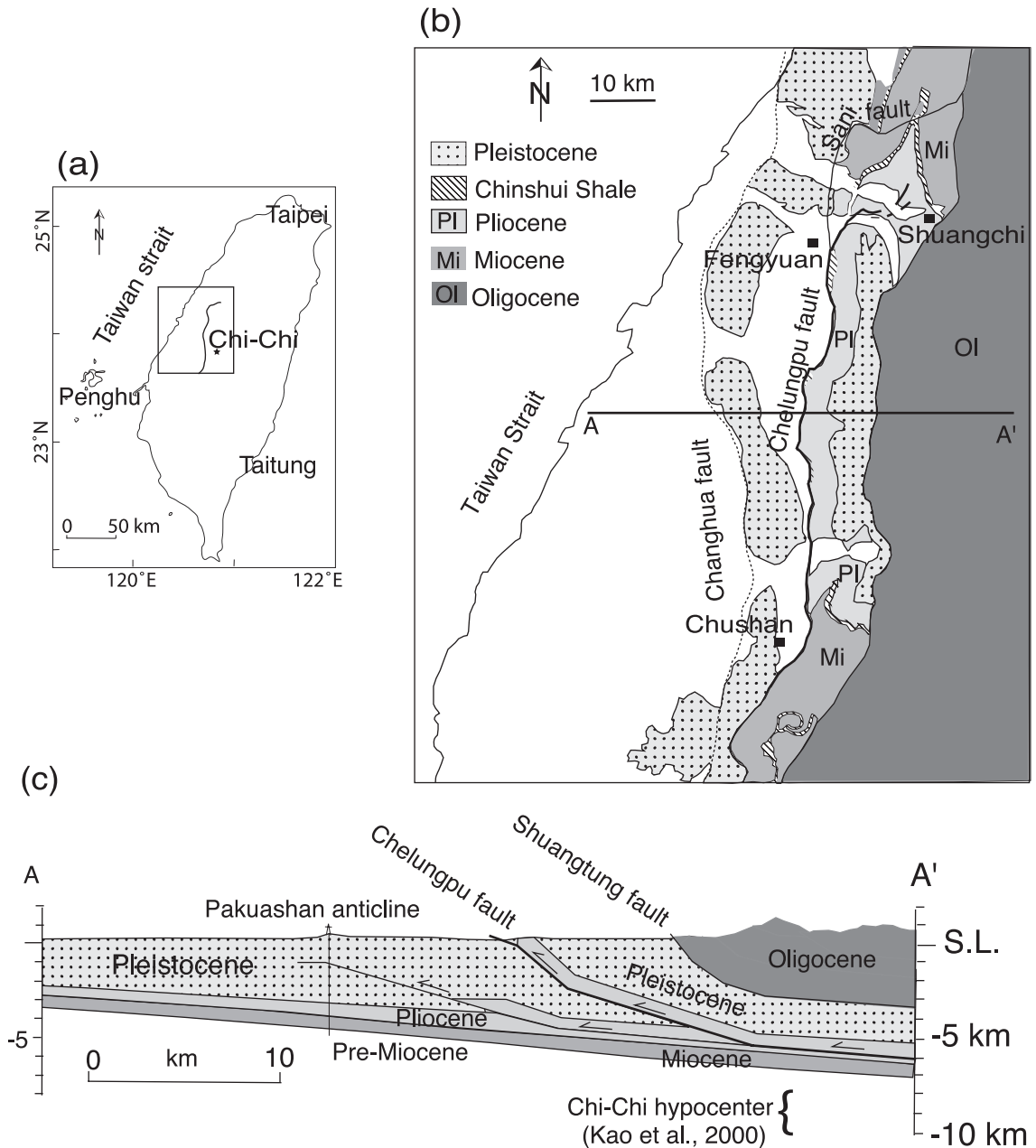
Fig. 1. (a) Location of Chi-Chi earthquake and ground ruptures in west-central Taiwan. (b) Simplified geologic map of west-central Taiwan. (c) Cross-section of Chelungpu fault (Suppe, 1987). Upper ramp of Chelungpu fault dips ~ 25° sand lower flat dips ~ 5°.

While the main features of the Chi-Chi earthquake ruptures, being based on independent field observations made by numerous investigators, are not in dispute, there is inconsistency in the literature regarding the subsurface shape of the fault that ruptured during the earthquake. One expression of the uncertainty in the fault shape is centered on the controversy over "thin-skinned" vs. "thick-skinned"

tectonics in Taiwan. The thin-skinned model for Taiwan tectonics originated in early studies of the structural geology (e.g., Suppe and Namson, 1979) in which it was supposed that ~ 30° dipping thrust faults soled into a shallow dipping décollement. Suppe (1987) proposed this fault geometry for the Chelungpu fault, based on dips of rock units at the ground surface and records of two boreholes that penetrate nearby thrust faults and a borehole on the coastal plane of western Taiwan (Fig. 1c). Suppe's cross-section shown in Fig. 1c shows the Chelungpu fault dipping east about 25° down to 5–6 km where the fault merges with a 5° dipping décollement. Davis et al. (1983) further developing the idea of ramp–décollement fault geometry in Taiwan, proposed a major décollement under the entire island of Taiwan that approximately coincides with this lower Chelungpu flat. Carena et al. (2001) used locations of small earthquakes to infer a sub-horizontal décollement at ~ 10 km depth under the western foothills and the central ranges. Two recently acquired seismic reflection profiles across the Chelungpu fault are consistent with this thin-skinned model (Hung and Suppe, 2002). Hung and Suppe interpret a 20–40° dipping ramp extending down to a décollement at 6 km depth in the north and 10 km depth in the south.

Other investigators have proposed that the Chelungpu fault and adjacent faults represent "thick-skinned" tectonics in which reverse faults extend to greater depths. For example, Wu et al. (1997) suggested "thick-skinned" tectonics in Taiwan on the basis of their analyses of seismic and gravity data. Their model lacks a major décollement above which the deformation is concentrated. Rather, Wu et al. (1997) suggest that the major reverse faults extend well below 10 km depth.

The notions of thin- and thick-skinned tectonics arose in Taiwan before the Chi-Chi earthquake and they influence various investigators' interpretations of the shape of the Chi-Chi earthquake fault at depth. Finite source modeling by numerous investigators, who have used strong ground motion and GPS data together with elastic dislocation theory, have estimated "thick-skinned" models on 20–30° dipping fault planes along the Chushan–Fengyuan section that extend to 15–20 km depths (Ji et al., 2001; Johnson et al., 2001; Ma et al., 2001; Wang et al., 2001; Wu et

al., 2001; Yoshioka, 2001; Zeng and Chen, 2001). For example, Fig. 2a is a three-dimensional view of the fault geometry and slip distribution estimated by Johnson et al. (2001).

Other investigators have assumed that coseismic slip occurred on ramp–décollement fault geometry. Loevenbruck et al. (2001) used GPS data to invert for slip assuming Suppe's (1987) ramp–décollement geometry. Wang et al. (2000) modified Suppe's (1987) fault geometry, assuming a décollement at 8 km depth, coinciding roughly with the hypocentral depth of the main shock. Chen et al. (2001a) inferred a sub-horizontal décollement from qualitative analysis of the vertical GPS displacements, suggesting the spatial extent of coseismic subsidence delineates the location of the horizontal décollement. Fig. 3 shows various proposed fault geometries for the Chelungpu fault.

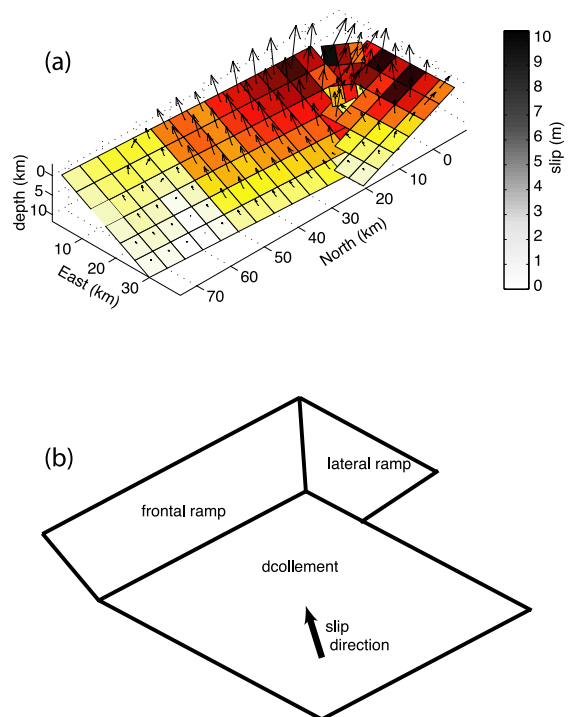One might hope that aftershocks could help resolve the debate over the geometry of the Chi-Chi earth-

Fig. 2. Curved fault model from Johnson et al. (2001). N–S trending fault plane dips 23°, extends to 12 km depth, and has reverse and left-lateral slip components. E–W lateral ramp at northern end dips 21° and has reverse and right-lateral slip components.
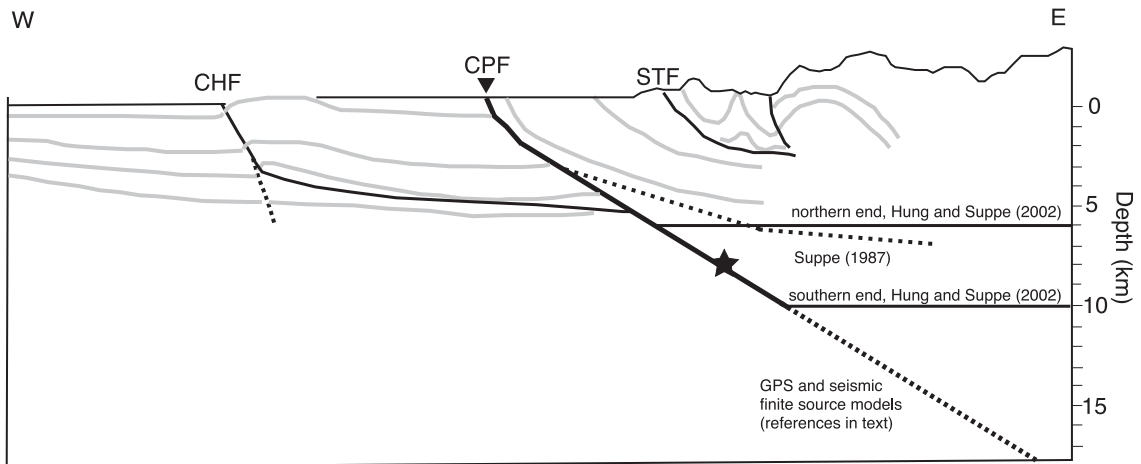
Fig. 3. Structural cross section across Chelungpu fault after Chen et al. (2001a). CHF, Changhua fault; CPF, Chelungpu fault; STF, Shuangtung fault. Upper dashed line is ramp-décollement inferred by Suppe (1987). Lower dashed line is the downward extension of the upper ramp assumed in most finite source inversions. Solid horizontal lines indicate décollement proposed by Hung and Suppe (2002). Star denotes 8 km depth of Chi-Chi earthquake.

quake fault surface. Aftershock distributions have been used in other large earthquakes to estimate the area of coseismic rupture (e.g., Mellors et al., 1997). This method, however, is not helpful for the Chi-Chi earthquake because there are clusters of aftershocks around the depth of the proposed décollement (~ 10 km) and down to 20 km at the location of the down-dip extension of the ~ 30° dipping ramp (Hirata et al., 2000).

One purpose of this paper is to determine whether coseismic slip occurred on a décollement or on the down-dip extension of the upper ramp. We use coseismic GPS data (Yu et al., 2001) to test the ramp–décollement hypothesis by investigating 3-D fault models that include both a ramp and décollement using well-established methods of inverting GPS data for fault geometry and slip distribution on faults represented by elastic dislocations.

Determining whether coseismic slip occurred on the Chelungpu décollement has important implications for studies of active deformation in Taiwan (e.g., Hsu et al., 2003). While the reflection profiles across the Chelungpu fault probably erase any doubt over whether the fault developed with ramp–flat geometry over much of the history of orogeny, the existence of a décollement does not belie the possibility that deformation has shifted from the décollement to the down-dip ramp extension. Thus, the

finite source models outlined above illustrate two distinct possibilities for the coseismic fault geometry of the Chi-Chi earthquake: slip on the down-dip extension of the Chelungpu ramp, or slip along the ramp and décollement. In each of the finite source inversions, the investigators assumed one of the two fault geometries and reported satisfactory fit to the data. Thus, these studies do not allow us to discern whether coseismic slip actually occurred on the décollement.

The second issue we address in this paper is the subsurface fault geometry beneath the northern end of the Chi-Chi earthquake rupture, where it leaves the north/south trend of the surface trace of the Che-lungpu fault and extends eastward about 10 km along the Fengyuan/Shuangchi segment (Fig. 1). Several authors have shown that the addition of a NE/SW or E/W striking fault plane at the northern termination (Fig. 2) improves the fit to GPS data (Johnson et al., 2001; Zeng and Chen, 2001; Yoshioka, 2001) and strong ground motion data (Ji et al., 2001; Ma et al., 2001; Wu et al., 2001). This fault geometry consists of an east-dipping frontal ramp that bends to the north into a south dipping lateral ramp. Frontal and lateral ramp–décollement geometry (Fig. 2b) was proposed for by Hung and Wiltschko (1993) for the bend in the Sani fault, which is the northern extension of the part of the Chelungpu fault that ruptured in the Chi-Chi

earthquake (Fig. 1). A difficulty with the lateral ramp interpretation for the 1999 earthquake is that there was no surface representation of slip on the lateral ramp. Mapping of surficial structures in the northern Chi-Chi fault zone by Lee et al. (2002) and others shows that the deformation consists of a series of discontinuous reverse faults and fold-scarps in a 3-km-wide zone. The surficial deformation does not clearly reflect a continuous, south dipping thrust fault. In this paper we will describe two alternate models for deformation at the northern end and test these models with coseismic GPS data.

In this paper, we show that the shape of the Chelungpu fault, as revealed by coseismic GPS displacements, is best characterized by a frontal and lateral ramp–décollement geometry as illustrated schematically in Fig. 2b.

2. Testing the décollement hypothesis

2.1. Homogeneous half-space model

To test the ramp–décollement hypothesis, we begin by ignoring heterogeneity in earth structure and assume the fault slipped in a homogeneous, isotropic, elastic half-space. To test for a change in dip of the fault at depth, we add a lower fault plane to our previous (Johnson et al., 2001) three-fault model to produce a four-fault model as shown in Fig. 4. We optimize seven parameters: the dips (δ_1, δ_2, δ_3, δ_4) of all four fault planes, the depth (D) to the connection of planes 1 and 4, and the strike (θ) and length (L) of fault 3. The fixed parameters were determined as follows: the length, strike, and depth to top (zero) of faults 1–3 were
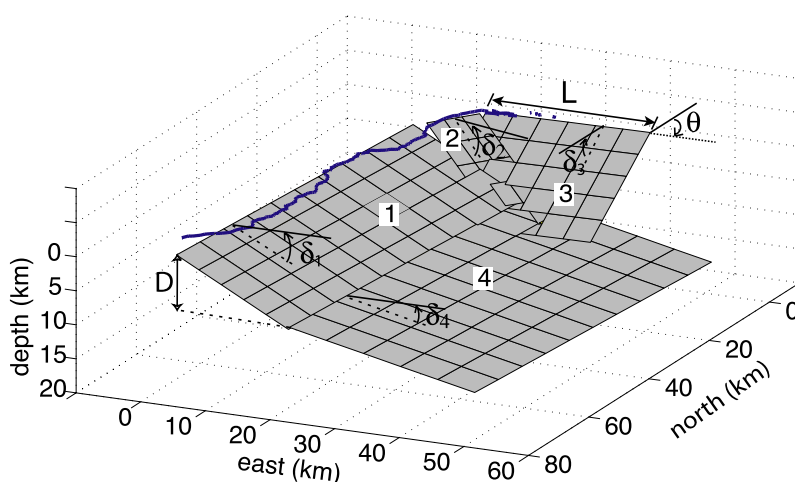
	δ_1	δ_2	δ_3	L	θ	δ_4	D
optimal value	26°	23°	23°	27 km	90°	0	7.7 km
95% confidence interval	22-31	13-30	14-41	22-35	49-94	0-7	5.8-8.6

Fig. 4. The seven optimized fault parameters and the uncertainties in the estimates: D, depth to upper edge of fault 4; δ_1, δ_2, δ_3, δ_4, dips of faults 1–4; L, length of fault 3; θ, strike of fault 3.

chosen to coincide with surface ruptures and their widths were determined by the depth to the décollement. The width of fault 4, the décollement, is arbitrary but was chosen to be wide enough that insignificant amounts of slip occurred at the eastern edge of the fault in the inversions. Furthermore, we constrained the dip of fault 4 to be greater than zero; that is, we do not allow fault 4 to be inclined up to the east. The seven fault parameters to be estimated are nonlinearly related to surface displacements, so we performed the inversion using Matlab's *lsqnonlin* optimization algorithm. In addition to the seven fault parameters, we also simultaneously inverted for the slip distribution on the fault planes (following the procedure in Johnson et al., 2001).

The optimal fault geometry is tabulated in Fig. 4 and shown in Fig. 5. The predicted horizontal and vertical displacements are compared with the measured displacements (Yu et al., 2001) in Figs. 6 and 7. Planes 1–3 dip 23–26°, slightly steeper than the 21–23° we reported for the three-fault model with no décollement (Johnson et al., 2001). Fault 3 strikes directly E/W as in the three-fault model, and the décollement is horizontal. Slip on the décollement is

significant as it contributes 21% of the total moment release in our model.

Uncertainties in the fault parameters (95% confidence) were computed with a bootstrap analysis (Efron and Tibshirani, 1993). Considering the uncertainties in the model parameters, the true depth to the western edge of the décollement lies somewhere in the range 5.8–8.6 km and the true dip is between 0° and 7°. The bootstrap uncertainties rule out, at 95% confidence, coseismic slip on the down-dip extension of the upper ramp.

The weighted root mean square misfit (Segall and Harris, 1986) for the décollement model is 0.16 m, which is well above the measurement uncertainties of several mm in the east and west and nearly 1 cm in the vertical. Yet, the model accounts for the overall pattern of deformation (Figs. 6 and 7). The weighted root mean square misfit for the décollement model is lower than the 0.19 m obtained for our earlier model that lacked a décollement (Johnson et al., 2001), but this is only a 16% improvement. Thus, the clearest indication of slip on the décollement as opposed to slip on the down-dip extension of the ramp is the bootstrap estimate of uncertainties.
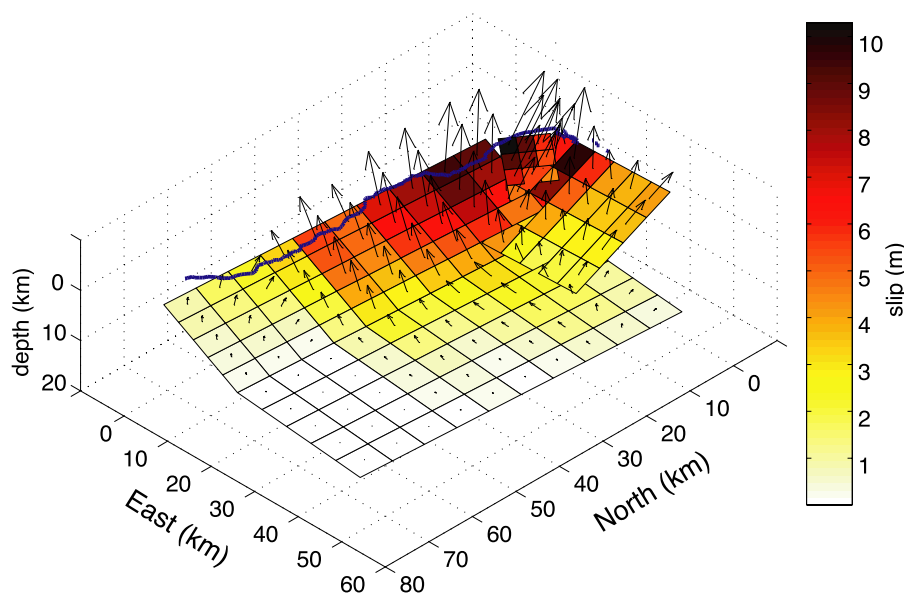

Fig. 5. Optimized fault geometry, assuming homogeneous earth model, with lateral ramp at northern end and sub-horizontal décollement at 7.7 km depth.
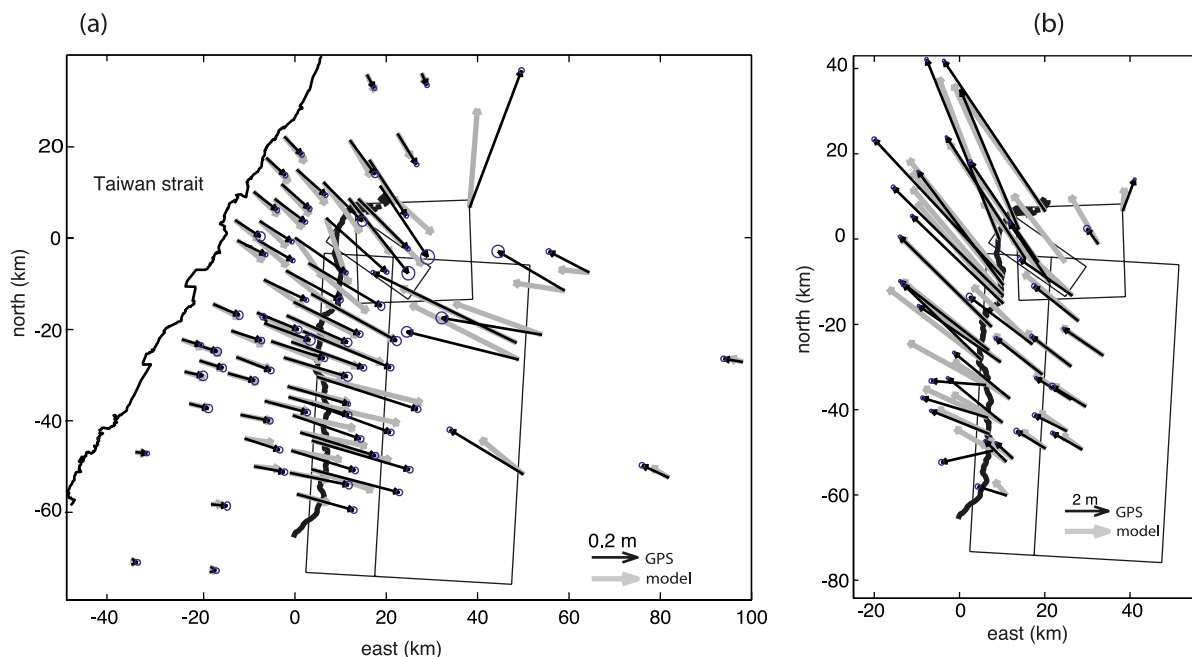
(a)

(b)

Fig. 6. Measured and modeled horizontal displacements. Ellipses are 2σ errors. (a) Footwall and far-field hangingwall displacements. (b) Hangingwall displacements. Note different scales.

2.2. Heterogeneous half-space model

It is uncertain, however, whether our estimate of the depth is biased by the assumption of a homogeneous, elastic earth. It is well known that ignoring heterogeneity can bias geodetic estimates of fault parameters. For example, Cattin et al. (1999) and Du et al. (1997) have shown that homogeneous half-space models underestimate the depths of buried thrust faults when shallow rocks have lower shear modulus than rocks at depth. Thus, we estimated the fault geometry and the depth of the décollement using a more nearly realistic earth model.

We use the p-wave velocity model of Cheng (2000) and the density model of Yen and Yeh (1998) to construct an idealized earth model for the Chi-Chi earthquake (Fig. 8c). An estimate of relative shear modulus can be obtained from the velocity and density models using the relationship $V_p = (3\mu/\rho)^{1/2}$, where μ is shear modulus and ρ density and Poisson's ratio is assumed to be 0.25. The increase in velocity and density from the ground surface to 30 km depth corresponds to a 140% increase in shear

modulus. Also the velocity contrast across the Chelungpu fault corresponds to a 17% increase in shear modulus from west to east. Thus, we construct an idealized earth model containing both lateral and vertical variations in shear moduli as shown in Fig. 8c. We also consider two earth models that ignore the lateral contrast in shear modulus as shown in Fig. 8d. The static response of the earth to sudden earthquake loading may result in effectively higher shear moduli contrasts than estimated from seismic data (e.g., Hooper et al., 2002). In addition to the earth modeling consisting of a 140% increase in shear modulus from the surface to 30 km depth, as estimated from seismic methods, we estimate the fault geometry with an earth model consisting of a 260% increase in shear modulus. We also check the effect of a soft, shallow sedimentary layer near the earth's surface. We construct a fourth heterogeneous model consisting of the same layers in the previously mentioned model with the 260% increase in shear modulus but with a 0.5-km-deep surface layer with relative shear modulus of 0.1 (factor of 10 softer than the top layer in Fig. 8d).
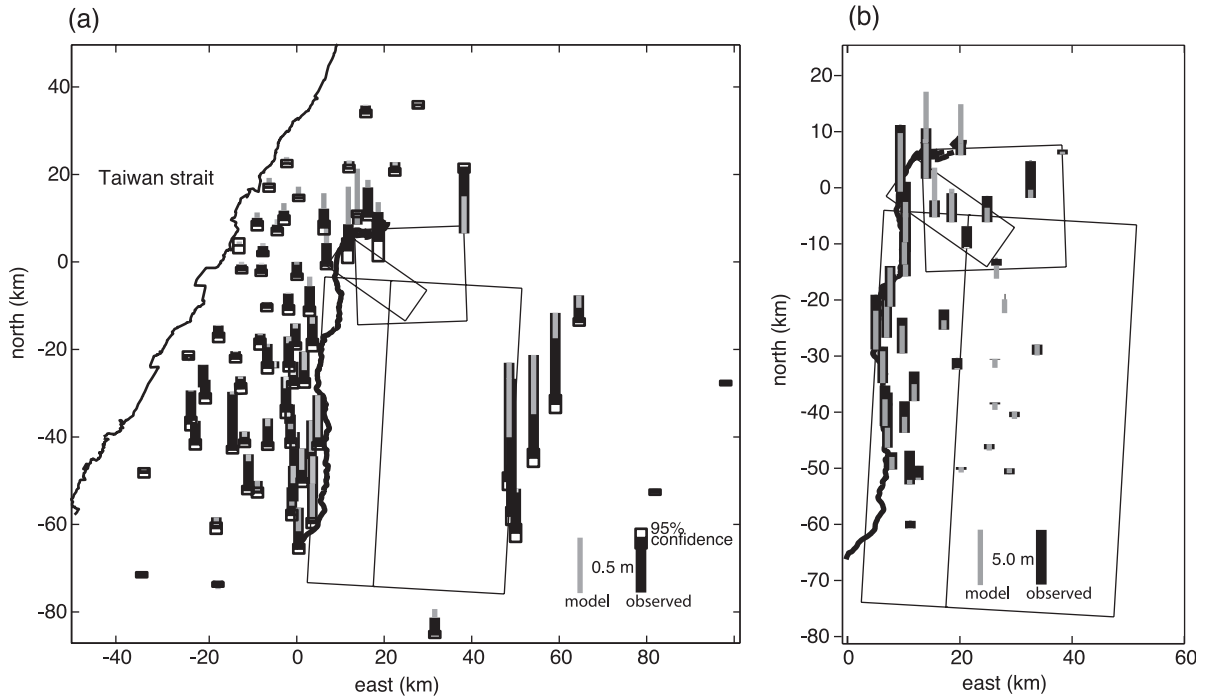
Fig. 7. Measured and modeled vertical displacements. (a) Footwall and far-field hangingwall displacements. (b) Hangingwall displacements. Uncertainties are too small to show at this scale. Note different scales.
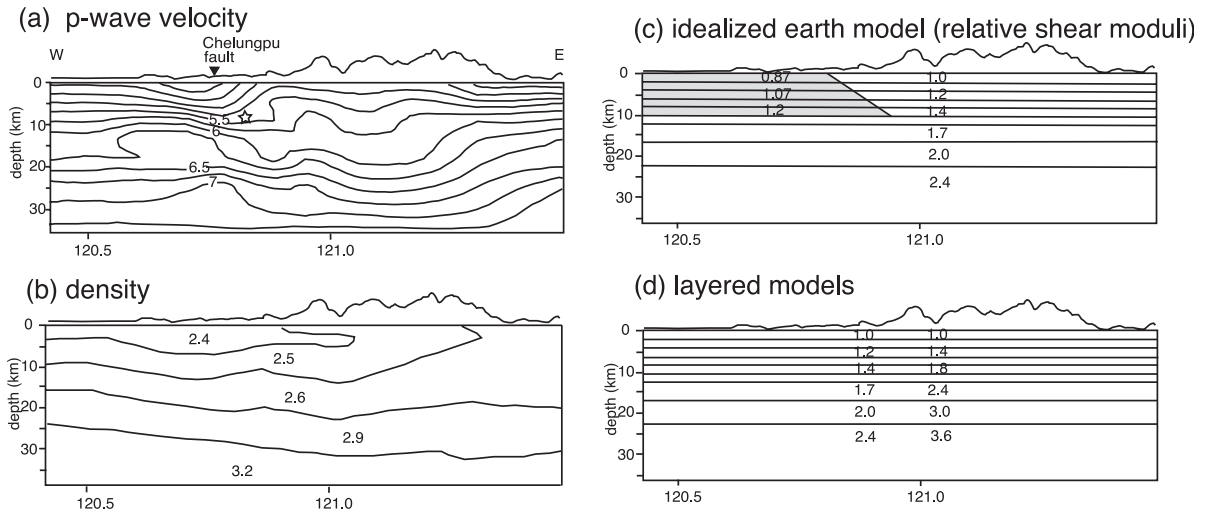

Fig. 8. (a) p-Wave velocity profile from Cheng (2000). Velocity in km/s. Note the contrast in velocity across the Chelungpu fault zone. (b) Density model from Yen and Yeh (1998). (c) Idealized earth model based on p-wave velocities and density. This is the earth model assumed in idealized, heterogeneous dislocation model containing lateral and vertical contrasts in shear moduli. Numbers give relative shear modulus in each layer (relative to upper layer). (d) Layered earth models. The two sets of shear moduli correspond to two different layered earth models used to estimate fault geometry.
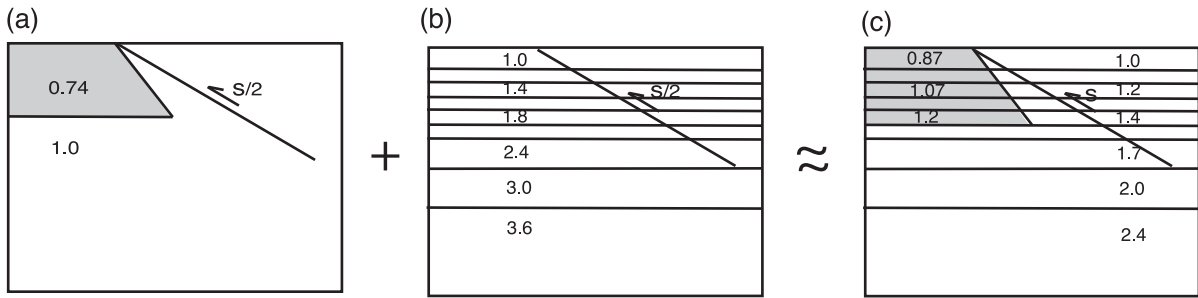
Fig. 9. Superposition of perturbation solution (a) and propagator matrix solution (b) to obtain an approximate solution for the fully heterogeneous earth model (c).

The effects of vertical variations in shear moduli have been determined with an application of the propagator matrix method (e.g., Sihng, 1970; Ward, 1985). It is an exact solution for a dislocation within a medium containing vertical contrasts. A first-order approximation for a dislocation in a medium with the lateral contrast is calculated using a perturbation method (Du et al., 1994,1997). Du et al. (1994) show that two first-order perturbation solutions can be superposed to obtain another valid first order perturbation solution. In this case the shear moduli in the overlapping regions are averaged in the superposed solution. This is not generally true for higher order perturbation approximations or exact solutions, however, we obtain an approximate solution containing lateral and vertical contrasts by perturbing the solution for a dislocation in a homogeneous half-space to obtain first order corrections for the lateral contrast in shear modulus, and then superpose this solution with an exact propagator matrix solution. This might be considered a slight improvement to using a perturbation approach to calculate both vertical and lateral contrasts in shear moduli, and furthermore this approach is much more computationally efficient. Fig. 9 demonstrates this procedure graphically.

With the heterogeneous model it is not computationally feasible to optimize seven fault parameters and estimate the uncertainties as we did with the homogeneous model, therefore we use the result from the homogeneous model of a horizontal décollement. In this case we estimate the depth to the décollement by scanning through a range of values for the depth, finding the value that minimizes the misfit to the data. Fig. 10 shows a misfit vs.

depth plot for all the earth models. The best-fitting model is the layered model with the soft surface layer with a depth of 8.4 km for the décollement.
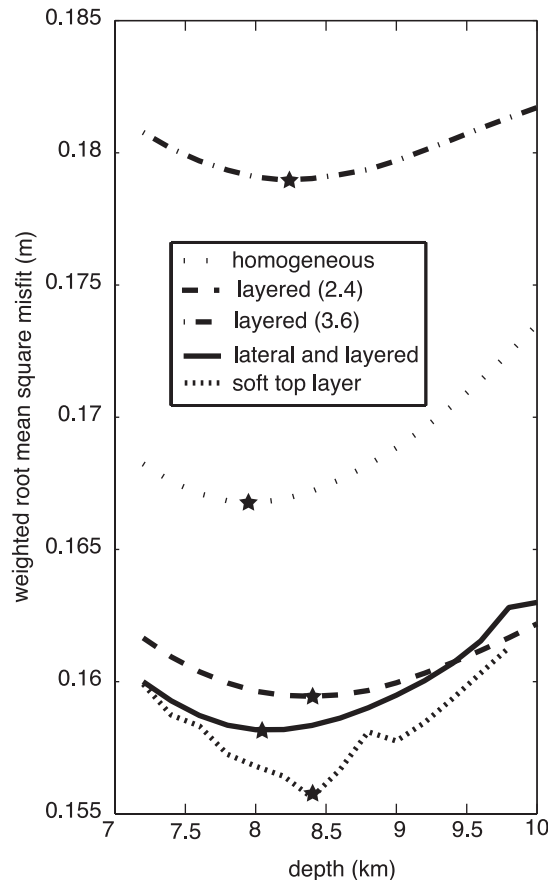

Fig. 10. Plots of root mean square misfit vs. depth to décollement for the four heterogeneous earth models and the homogeneous earth model. Minimum misfit denoted with star.

Notice that the earth model does not largely influence the depth to the décollement. The décollement depth is in the range 8–8.4 km for all of the earth models. Because of the computational expense, we did not estimate bootstrap confidence intervals for the heterogeneous solutions. However, if we assume the range in uncertainties in depth is similar to the range obtained for the homogeneous model, the true depth to the décollement lies somewhere in the range 6.1–8.9 km.

2.3. Discussion of results for lower décollement

We conclude that coseismic slip occurred on a sub-horizontal décollement at about 6–9 km depth. Our inversions rule out, at 95% confidence, coseismic slip on a downward extension of the ~30° dipping upper ramp. Seismic reflection profiles across the Chelungpu fault reveal a décollement at 6 km depth in the north and 10 km in the south (Hung and Suppe, 2002). It is likely that the model décollement at 6–9 km depth is an "averaged" image of the variable depth décollement revealed in the reflection profile that shallows from 10 km in the south to 6 km in the north. Thus, we claim that our result is consistent with slip on the Chelungpu fault with ramp–décollement geometry proposed by Hung and Suppe (2002).

Independent evidence of slip on the décollement is reported by Hsu et al. (2002). The authors use GPS measurements in the 3 months following the Chi-Chi earthquake to show that afterslip likely occurred on a sub-horizontal décollement estimated from the data at 8–12 km depth.

3. Analysis of deformation at northern end of Chi-Chi rupture

Whereas the east-dipping frontal ramp and the sub-horizontal décollement we have imaged from GPS data are consistent with the seismic reflection profiles and present theories of thin-skinned tectonics in western Taiwan, it is less clear how the lateral ramp of the Chi-Chi earthquake rupture fits in with the geologic setting near the northern end of Chelungpu fault. The simplified geologic map in Fig. 1 shows that the Chi-Chi fault rupture deviates from the trend of the Chelungpu fault near Fengyuan and cuts eastward across the axis of a regional syncline (hereafter called the Shihkang syncline). Fig. 11 shows these terminating ground ruptures in more detail.

In this northern area the ground ruptures branch into a 3 km wide zone of discontinuous, north and south dipping reverse faults that occurred along
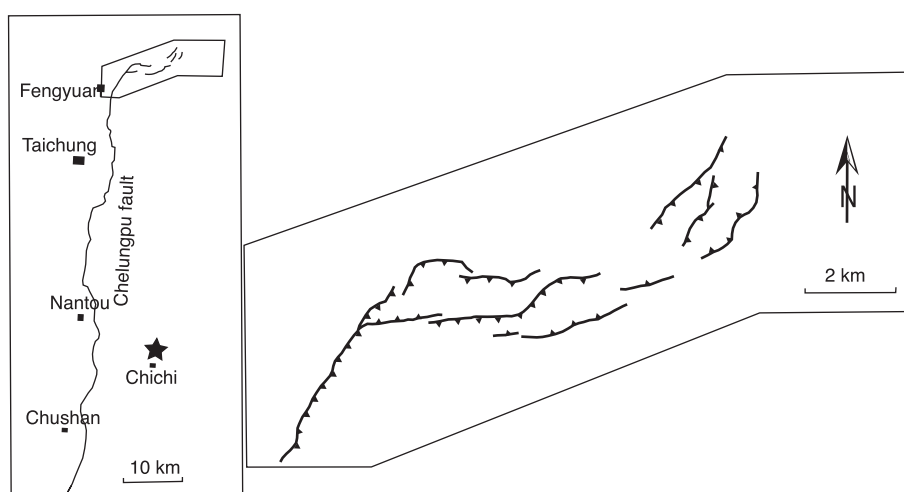

Fig. 11. Map of discontinuous thrust faults in northern fault zone after Lee et al. (2002).

reactivated preexisting geologic structures. The structures that Lee et al. (2002) describe in this area do not appear to be the surface expressions of the south-dipping lateral ramp that we have included in our model. Thus, it might appear that the lateral ramp at the northern end is inconsistent with the mapped geology. There are at least two conceivable alternative models for deformation in the northern fault zone that are consistent with observations of surface geology and do not require the large E−W fault cutting through the Shihkang syncline. We will describe these two models and test them against the GPS data.

3.1. Shallow faults in northern fault zone

The simplest explanation for deformation in the northern fault zone is slip confined to the mapped faults in the complex northern fault zone. These relatively short rupture segments followed preexisting, localized topographic features (Lee et al., 2002). Thus, it is possible that all of the deformation at the northern end occurred as slip on shallow faults underlying these preexisting features. This hypothesis is easy to test for consistency with the GPS data. We removed the lateral ramp in our model (Fig. 5) and replaced it with four smaller fault segments that coincide roughly with the mapped fault segments (Fig. 12a). Each of the four fault segments dips 45° and extends to 1 km depth (the 1 km depth was chosen so that the down-dip width of each fault segment is comparable to the length). We held the geometry of the seven faults fixed (four shallow faults and the three faults remaining from the model in Fig. 6) and inverted for slip on the seven fault surfaces. Fig. 12a shows that this model does not fit the GPS observations at stations north of the E/W fault zone, and furthermore, the inversion places unreasonably large amounts of slip (>100 m) on parts of the shallow faults. In fact, the predicted displacements at stations M553, G096 and G097 are oriented entirely in the wrong direction. For comparison, note in Fig. 12b that our optimized fault model with the large south-dipping ramp much better predicts the displacements at these stations. Therefore, based on the inconsistency with the GPS data, we feel that we can confidently rule out slip on shallow mapped faults as the sole source of deformation below the northern fault zone.
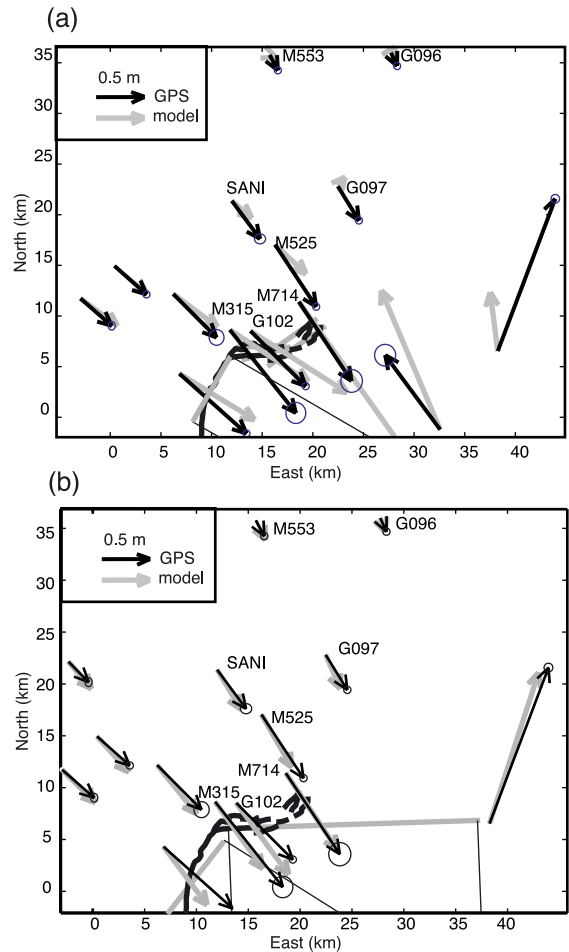

Fig. 12. (a) Close-up view of horizontal displacements north of northern fault zone. A. Faults in northern fault zone are modeled as four 45° dipping faults extending from ground surface to 1 km depth. We inverted for slip on each of the four faults and the frontal ramp and décollement. Note the modeled displacements at stations M553, G096, SANI, and G097 do not fit the GPS data. (b) Same as (a) for the optimized fault geometry with 27-km-long northern lateral ramp.

3.2. Slip confined to Chinshui shale

Another conceptual model of deformation that can be reconciled with the regional geology at the northern end was proposed by Lee et al. (1999, 2002). These authors suggest that slip was confined at depth to a fault surface in the Chinshui shale. The Chinshui shale outcrops along the trace of the Chelungpu fault in the Chushan−Fengyuan section (Fig. 1) and dips

approximately parallel to the Chelungpu fault. Thus, it has been proposed that the Chelungpu fault is bed-parallel fault within the Chinshui shale. At the northern end of the Chelungpu fault the Chinshui shale is folded in the Shihkang syncline. Since the fault appears to dip parallel to the Chinshui shale south of the syncline, it seems plausible that slip occurred along the curved Chinshui shale surface in the Shihkang syncline. Fig. 13 shows the structural contours of the base of the Chinshui shale along the Chelungpu fault and within the Shihkang syncline. The cross-section of Lee et al. (1999) shows slip confined to the Chinshui shale for much of the length of the profile before the fault breaks up through section and to the ground surface at the northern end where the Chinshui shale flattens out at the top of the syncline. These

authors suggest that the surface deformation within the northern fault zone is related to slip within the folded Chinshui shale.

To test this conceptual model for consistency with the GPS data, we have approximated the proposed Chinshui shale fault surface with two faults as shown in Fig. 14a. The faults were chosen to roughly coincide with the shape of the Chinshui shale within the syncline. Note that this geometry is similar to the lateral ramp geometry in Fig. 5, except the northern fault is only 10 km long. We also include two small fault segments that coincide with the ground ruptures trending NE just south of station M714 (Fig. 12). We keep the upper ramp and lower décollement as in Fig. 5 and invert for slip on the six fault surfaces.

Fig. 14a shows the predicted displacements for this model. As is the case with the model in the previous section, the displacements do not fit at the stations north of the fault. In particular, stations G097, G096, and M553 are grossly underfit by the model. For comparison we show the fit to the data if the northern fault is extended to 27 km length as in Fig. 5. It is clear that the northern lateral ramp must extend well beyond the width of the Shihkang syncline in order to fit the GPS data. Thus, slip confined to the Chinshui shale in the syncline is inconsistent with the GPS data.

3.3. Discussion of analysis of deformation in northern fault zone

We have shown that the two models of the northern Chi-Chi earthquake rupture, which restrict the deformation to the length of the E/W trending fault zone, produce displacements that are in fact inconsistent with the GPS measurements. It seems that the inconsistency with the GPS data arises because slip on faults constrained to the Shihkang syncline do not provide the lateral extent of the source of deformation needed to fit the significant displacements located as far as 30 km north of the northern fault zone. This result is reflected in the 95% confidence interval for the estimated length of the northern fault (Fig. 4). According to the bootstrap estimate of uncertainties of this parameter (Efron and Tibshirani, 1993), the minimum length for this fault segment is 22 km, about twice the width of the syncline.
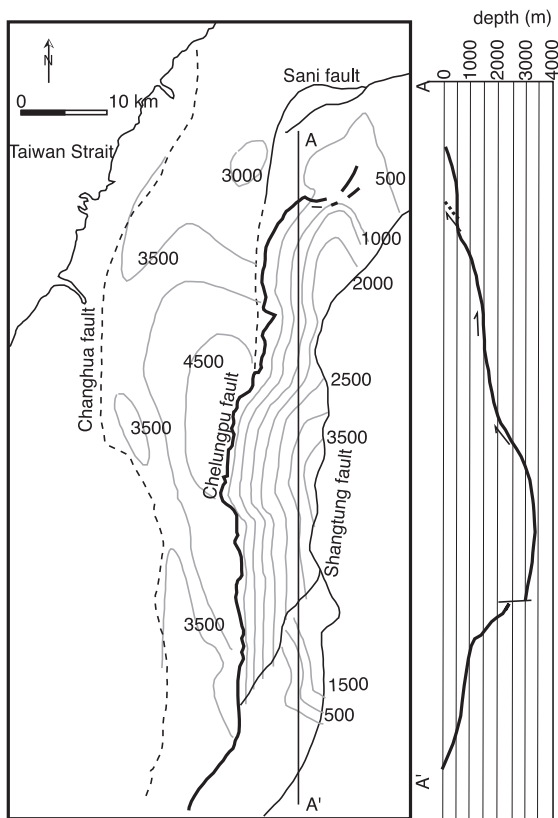

Fig. 13. Structural contour map of Chinshui shale (Lee et al., 1999) showing the unit folded into a syncline at the northern end. Lee et al. (1999) suggest that coseismic slip occurred on a fault within the Chinshui shale and surfaced within the northern fault zone.

(a) 10 km long lateral ramp

Fig. 15. (a) Focal mechanism from synthetic moment tensor for 10-km-long lateral ramp. (b) Focal mechanism from synthetic moment tensor for 27-km-long lateral ramp. (c) Harvard CMT solution.
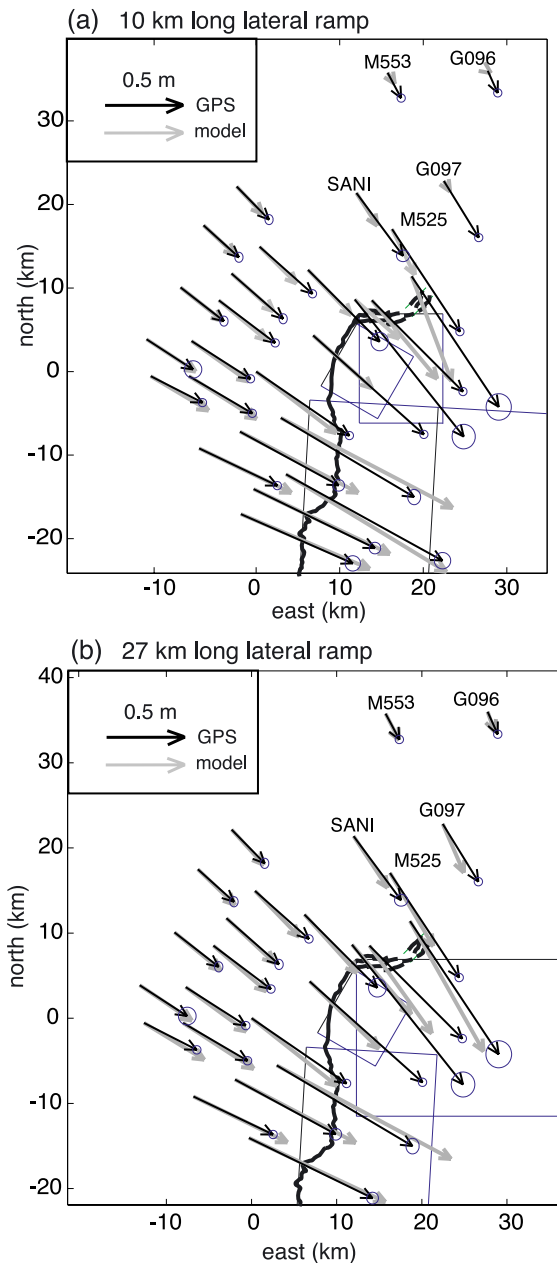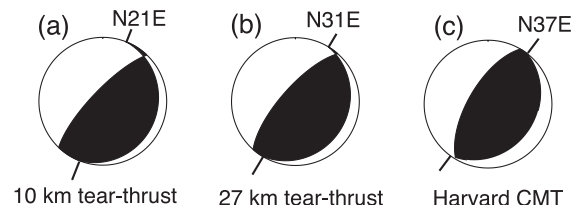
(b) 27 km long lateral ramp

Fig. 14. (a) Model consisting of faults in Shihkang syncline conformable (approximately) with the shape of the Chinshui shale. Northern fault segment does not extend beyond the width of the syncline. Modeled and measured horizontal displacements at stations north of northern fault zone. Note the poor fit. (b) Same as (a) for the optimized fault geometry with 27-km-long northern lateral ramp.

Coseismic slip on an ∼ 27-km-long lateral ramp is supported by long-period CMT solutions. Fig. 15 shows the Harvard CMT solution with two synthetic moment tensors calculated from our geodetic model. The total synthetic moment tensor is simply the sum of moment tensors calculated for each patch of slip in our model (e.g., Jost and Herrmann, 1989, Eqs. (17) and (18)). The focal mechanism plot displays the best-fitting double couple to the synthetic moment tensor. The primary fault plane of the focal mechanism for the 27-km-long lateral ramp is oriented similarly to the primary fault plane of the CMT mechanism. The primary fault plane for the model with the 10-km-long lateral ramp is oriented 16° to the north of the CMT solution. Thus, the 10-km-lateral ramp model does not produce enough moment on the lateral ramp to reproduce the seismic moment tensor. In addition, Kao and Chen (2000) show that the primary fault plane of sub-events of the mainshock progressively rotated from N/S to NE/SW as the rupture propagated to the north, also suggesting the northern lateral ramp ruptured coseismically.

A possible objection to the 27-km-long northern lateral ramp is that there was no fresh fault exposed at the ground surface, except possibly within 5 km east of the N–S rupture. We could, however, have obtained essentially the same results by extending the lateral ramp near to the surface, but not breaking the surface. The actual breakage of the surface does not markedly affect displacements far from the fault. We in fact do not have enough GPS data in the vicinity of the upper edge of the lateral ramp to resolve these details. A lateral ramp that is blind along much of its length explains both the lack of surface expression of this fault and the large GPS displacements 30 km to the north.

This certainly is not the first identification of a lateral ramp along the Chelungpu fault. Faults similar to the one imaged here have been mapped at the northern end of the Shihkang syncline. Chen et al. (2001b) show the N/S striking Chelungpu fault (often indicated as the Sani fault at this location) and the sub-parallel Holi fault abruptly change strike to nearly E/W, forming overthrusts. Furthermore, Chen et al. (2001b) cite evidence that these overthrusts are progressively younger from north to south. As mentioned in the Introduction, Hung and Wiltschko (1993) proposed a similar fault geometry for the Sani fault based on numerous retrodeformable cross-sections.

We propose a simple model for the formation of the lateral ramps along the Chelungpu/Sani fault in the context of Taiwan tectonics. Taiwan is located within the collision zone of the Philippine Sea plate and Eurasian plate and is forming in response to N50°W relative convergence. While the trend of the major east-dipping reverse faults in Taiwan is generally perpendicular to the relative convergence direction, the N/S trending portion of the Chelungpu fault that ruptured during the Chi-Chi earthquake is oblique to this direction. We suppose, for the sake of argument, that long-term slip on this portion of the Chelungpu fault is oblique and roughly in the direction of relative convergence. Indeed, this supposition is consistent with the oblique slip observed on the N/S frontal ramp in the Chi-Chi earthquake. We suggest that this oblique motion could generate lateral ramps over many earthquakes. To see that this is reasonable, we turn to a simple elastic dislocation model to estimate the strains at the northern end of the Chelungpu fault due to repeated slip over numerous earthquake cycles. We model coseismic slip on the frontal ramp with uniform slip on a rectangular dislocation in an elastic half-space (Okada, 1985). We assume uniform reverse/left-lateral slip in the direction of relative plate convergence on a 100-km-long, 30-km-wide, 30° east-dipping fault with northern termination at the Sani overthrust. Fig. 16a shows the principal directions of the elastic strains at the ground surface. We do not attempt to model absolute magnitudes of strain, so we apply an arbitrary amount of slip and consider only relative magnitudes of strain and the principal strain directions. For simplicity in presentation we
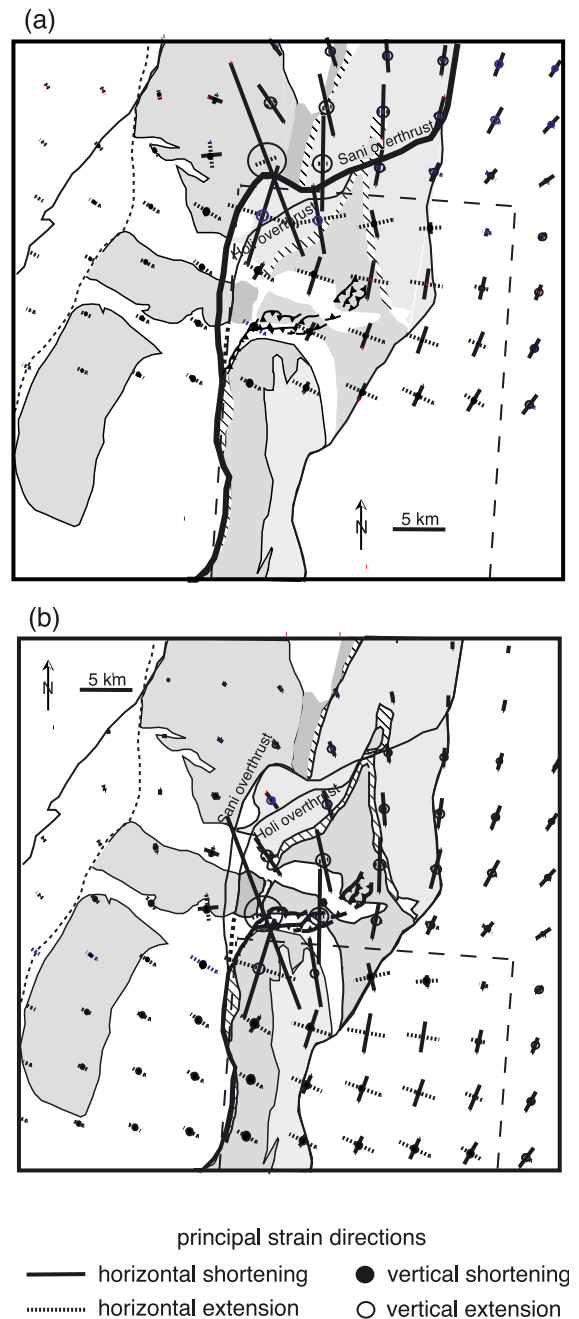

Fig. 16. Principal strains at ground surface due to oblique slip on Chelungpu fault. (a) Long-term slip extends to Sani overthrust. Sani overthrust forms in region of N/S shortening and vertical extension. (b) Long-term slip extends to end of Chi-Chi earthquake ruptures. E/W lateral ramp and northern fault zone occurs in region of N/S shortening and vertical extension.

show only the strains at the ground surface since the free surface condition guarantees that one infinitesimal principal strain (or stress) direction is vertical. The pattern of principal strains is similar below the ground surface. Note that oblique slip produces horizontal strike-parallel compression and vertical extension above the northern edge of the fault. These strains promote E–W oriented reverse faults, consistent with the south-dipping Sani overthrust. One might take this analysis a step further and propose that the northern extent of oblique slip, and therefore the region of N/S compression, is migrating southward with time, producing the progressive formation of the Sani, Holi and Chelungpu lateral ramps from north to south (Fig. 16). Notice further that the region of largest N/S shortening and vertical extension in Fig. 16b correlates spatially with the E/W trending reverse faults in the northern fault zone.

Thus, with this scheme we have a simple model that accounts for the existence of the lateral ramps and the faulting within the northern fault zone. This simple elastic model is by no means intended to be a complete analysis of the process responsible for the formation of lateral ramps in central Taiwan. Over long time periods, the deformation is clearly inelastic. Furthermore, this model only considers coseismic motion on the frontal ramp and ignores interseismic strain and any deformation not associated with slip on the frontal ramp. Yet, this simple model quantitatively illustrates the point that oblique motion on the Chelungpu/Sani fault may generate lateral ramps.

The north-to-south progression of deformation with time is consistent with the theory that orogen growth in Taiwan is migrating southwestward with time as oblique collision with the Luzon arc migrates (Suppe, 1984). The fact that relative velocities in Taiwan are higher in the southern half of the island suggests that there may deformation in central Taiwan attributable to the transition from high strain rates in the south to low strain rates in the north. Indeed, Chang et al. (2003) show a change in orientation of the maximum shortening direction from WNW to NNW (and locally NS) at the latitude of the northern end of the Chelungpu fault. The east–west lateral ramps may be a manifestation of this transition.

4. Conclusions

We have further modeled the GPS data from the 1999 Chi-Chi earthquake using a new, more nearly realistic earth model consisting of vertical and lateral elastic heterogeneity. Based on these new analyses, our best estimate of the structure of the 1999 Chi-Chi earthquake rupture in Taiwan is a ramp–décollement system with a lateral ramp at the northern end. We have imaged a $22–31°$ dipping upper ramp and sub-horizontal décollement at $6.1–8.9$ km depth with significant amounts of coseismic slip (21% of the total estimated moment release).

A 22- to 35-km-long, E/W-trending lateral ramp at the northern end of the Chi-Chi rupture is necessary to fit the GPS data. While there is no surface representation of this lateral ramp, hypotheses assuming deformation is restricted to the northern fault zone delineated by surface rupture cannot explain the GPS observations north of the Chi-Chi rupture. A simple dislocation model of repeated episodes of oblique slip on the Chelungpu fault is able to explain the development of the lateral ramp and faults with similar geometry to the north, the Sani and Holi overthrusts. In this model, long-term oblique slip on the Chelungpu fault produces strains at the northern end that are compatible with lateral ramp formation.

References

Carena, S., Suppe, J., Koa, H., 2001. Imaging the main décollement under Taiwan: implications for the critical-taper mechanics and large-scale topography. EOS Transactions AGU 82 (47), 1176.

Cattin, R., Briole, P., Lyon-Caen, H., Bernard, P., Pinettes, P., 1999. Effects of superficial layers on coseismic displacements for a dip-slip fault and geophysical implications. Geophysical Research International 137, 149–158.

Chang, C.P., Chang, T.Y., Angelier, J., Kao, H., Lee, J.C., Yu, S.B., 2003. Strain and stress field in Taiwan oblique convergent system: constraints from GPS observation and tectonic data. Earth and Planetary Science Letters 214, 115–127.

Chen, W.S., Huang, B.S., Chen, Y.G., Lee, Y.H., Yang, C.N., Lo, C.H., Chang, H.C., Sung, Q.C., Huang, N.W., Lin, C.C., Sung, S.H., Lee, K.J., 2001a. 1999 Chi-Chi earthquake: a case study on the role of thrust-ramp structures for generating earthquakes. Bulletin of the Seismological Society of America 91 (5), 986–994.

Chen, Y.G., Chen, W.S., Lee, J.C., Lee, Y.H., Lee, C.T., Chang, H.C., Lo, C.H., 2001b. Surface rupture of 1999 Chi-Chi earthquake yields insights on active tectonics of central Taiwan. Bulletin of the Seismological Society of America 91 (5), 977–985.

Cheng, W.B., 2000. Three-dimensional crustal structure around the source area of the 1999 Chi-Chi earthquake in Taiwan and its relation to the aftershock locations. Terrestrial, Atmospheric, and Oceanic Studies (TAO) 11 (3), 643–660.

Davis, D., Suppe, J., Dahlen, F.A., 1983. Mechanics of fold-and-thrust belts and accretionary wedges. Journal of Geophysical Research 88, 1153–1172.

Du, Y., Segall, P., Gao, H., 1994. Dislocations in inhomogeneous media via a moduli perturbation approach; general formulation and two-dimensional solutions. Journal of Geophysical Research 99, 13767–13779.

Du, Y., Segall, P., Gao, H., 1997. Quasi-static dislocations in three-dimensional inhomogeneous media. Geophysical Research Letters 24, 2347–2350.

Efron, B., Tibshirani, R.J., 1993. An Introduction to the Bootstrap Chapman & Hall, New York. 436 pp.

Hirata, N., Sakai, S., Liaw, Z.S., Tsai, Y.B., Yu, S.B., 2000. Aftershock observations of the 1999 Chi-Chi, Taiwan earthquake. Bulletin of the Earthquake Research Institute, Tokyo 75, 33–46.

Hooper, A, Segall, P., Johnson, K., Rubinstein, J., 2002. Reconciling seismic and geodetic models of the 1989 Kilauea south flank earthquake. Geophysical Research Letters, 10.1029/2002GL016156 26 (November 2002).

Hsu, Y.J., Bechor, N., Segall, P., Yu, S.B., Ma, K.F., 2002. Rapid afterslip following the 1999 Chi-Chi, Taiwan earthquake. Geophysical Research Letters 29, 1-1–1-4.

Hsu, Y.J., Simons, M., Yu, S.B., Kuo, L.C., Chen, H.Y., 2003. A two-dimensional dislocation model for interseismic deformation of the Taiwan mountain belt. Earth and Planetary Science Letters 211, 287–294.

Hung, J.H., Suppe, J., 2002. Subsurface geometry of the Sani–Chelungpu faults and fold scarp formation in the 1999 Chi-Chi Taiwan earthquake. EOS Transactions AGU 83 (47) (Fall Meet. Suppl., Abstract T61B-1268).

Hung, J.H., Wiltschko, D.V., 1993. Structure and kinematics of arcuate thrust faults in the Miaoli–Cholan area of western Taiwan. Petroleum Geology of Taiwan 28, 59–96.

Ji, C., Helmberger, D.V., Song, T.A., Ma, K.F., Wald, D.J., 2001. Slip distribution and tectonic implication of the 1999 Chi-Chi, Taiwan, earthquake. Geophysical Research Letters 28 (23), 4379–4382.

Johnson, K.M, Hsu, Y.J., Segall, P., Yu, S.B., 2001. Fault geometry and slip distribution of the 1999 Chi-Chi, Taiwan earthquake

imaged from inversion of GPS data. Geophysical Research Letters 28 (11), 2285–2288.

Jost, M.L., Herrmann, R.B., 1989. A student's guide to and review of moment tensors. Seismological Research Letters 60, 37–57.

Kao, H., Chen, W.P., 2000. The Chi-Chi earthquake sequence: active, out-of-sequence thrust faulting in Taiwan. Science 288, 2346–2349.

Kao, H., Chen, R.Y., Chang, C.H., 2000. Exactly where does the 1999 Chi-Chi earthquake in Taiwan nucleate? Hypocenter relocation using the master station method. Terrestrial, Atmospheric and Oceanic Sciences 11, 567–580.

Lee, Y.H., Wu, W.Y., Shih, T.S., Lu, S.T, Shieh, M.L., Cheng, H.C., 1999. 921 Chi-Chi earthquake surface deformation features—North of Beifung bridge. Central Geological Survey Special Publication No. 12, Special Issue for the Chi-Chi earthquake, 17–60.

Lee, J.C., Chu, H.T., Angelier, J., Chan, Y.C., Hu, J.C., Lu, C.Y., Rau, R.J., 2002. Geometry and structure of northern surface ruptures of the 1999 M_w = 7.6 Chi-Chi Taiwan earthquake: influence from inherited fold belt structures. Journal of Structural Geology 24, 173–192.

Loevenbruck, A., Cattin, R., Le Pichon, X., Courty, M.-L., Yu, M.-L., 2001. Seismic cycle in Taiwan derived from GPS measurements. Earth and Planetary Sciences 333, 57–64.

Ma, K.F., Mori, J., Lee, S.J., Yu, S.B., 2001. Spatial and temporal distribution of slip for the 1999 Chi-Chi, Taiwan, earthquake. Bulletin of the Seismological Society of America 91 (5), 1069–1087.

Mellors, R.J., Vernon, F.L., Pavlis, G.L., Abers, G.A., Hamburger, M.W., Ghose, S., Iliasov, B., 1997. The M_s = 7.3 1992 Suusamyr, Kyrgyzstan, earthquake: 1. Constraints on fault geometry and source parameters based on aftershocks and body-wave modeling. Bulletin of the Seismological Society of America 87, 11–22.

Okada, Y., 1985. Surface displacements due to shear and tensile faults in a half-space. Bulletin Seismological Society of America 75, 1135–1154.

Segall, P., Harris, R., 1986. Slip deficit on the San Andreas fault at Parkfield, California, as revealed by inversion of geodetic data. Science 233, 1409–1413.

Sihng, S.J., 1970. Static deformation of a multilayered half-space by internal sources. Journal of Geophysical Research 75, 3257–3263.

Suppe, J., 1984. Kinematics of arc–continent collision, flipping of subduction and back-arc spreading near Taiwan. Memoirs of Geological Society of China 6, 21–33.

Suppe, J., 1987. The active Taiwan mountain belt. In: Schaer, J.P., Rodgers, J. (Eds.), Anatomy of Mountain Chains. Princeton Univ. Press, Princeton, NJ, pp. 277–293.

Suppe, J., Namson, J., 1979. Fault-bend origin of frontal folds of the western Taiwan fold-and-thrust belt. Petroleum Geology of Taiwan 16, 1–18.

Wang, C.Y., Chang, C.H., Yen, H.Y., 2000. An interpretation of the 1999 Chi-Chi earthquake in Taiwan based on the thin-skinned thrust model. Terrestrial, Atmospheric and Oceanic Sciences 11 (3), 609–630.

Wang, W.H., Chang, S.H., Chen, C.H., 2001. Fault slip inverted from surface displacements during the 1999 Chi-Chi, Taiwan

earthquake. Bulletin of the Seismological Society of America 91 (5), 1167–1181.

Ward, S.N., 1985. Quasi-static propagator matrices; creep on strike-slip faults. Tectonophysics 120, 83–106.

Wu, F.T., Rau, R.J., Slazberg, D., 1997. Taiwan orogeny: thin-skinned or lithospheric collision? Tectonophysics 274, 191–220.

Wu, C., Takeo, M., Ide, S., 2001. Source process of the Chi-Chi earthquake: a joint inversion of strong motion data and global positioning system data with multifault model. Bulletin of the Seismological Society of America 91 (5), 1128–1143.

Yen, H.Y., Yeh, Y.H., 1998. Two-dimensional crustal structures of Taiwan from gravity data. Tectonics 17, 104–111.

Yoshioka, S., 2001. Coseismic slip distribution of the 1999 Chi-Chi, Taiwan, earthquake deduced from inversion analysis of GPS data. Bulletin of the Seismological Society of America 91 (5), 1182–1189.

Yu, S.B., Kuo, L.C., Hsu, Y.J., Su, H.H., Lui, C.C., Hou, C.S., Lee, J.F., Lai, T.C., Liu, C.C., Liu, C.L., Tseng, T.F., Tsai, C.S., Shin, T.C., 2001. Preseismic deformation and coseismic displacements associated with the 1999 Chi-Chi, Taiwan, earthquake. Bulletin of the Seismological Society of America 91, 995–1012.

Zeng, Y., Chen, C.H., 2001. Fault rupture process of the 20 September 1999 Chi-Chi, Taiwan, earthquake. Bulletin of the Seismological Society of America 91 (5), 1088–1098.